JPE 16-5-35

http://dx.doi.org/10.6113/JPE.2016.16.5.1981
ISSN(Print): 1598-2092 / ISSN(Online): 2093-4718

Development of an Intelligent Charger with a Battery Diagnosis Function Using Online Impedance Spectroscopy

Thanh-Tuan Nguyen*, Van-Tuan Doan*, Geun-Hong Lee*, Hyung-Won Kim*, Woojin Choi†, and Dae-Wook Kim**

*,†Department of Electrical Engineering, Soongsil University, Seoul, Korea
** Department of Economics, Soongsil University, Seoul, Korea

Abstract

Battery diagnosis is vital to battery-based applications because it ensures system reliability by avoiding battery failure. This paper presents a novel intelligent battery charger with an online diagnosis function to circumvent interruptions in system operation. The charger operates in normal charging and diagnosing modes. The diagnosis function is performed with the impedance spectroscopy technique, which is achieved by injecting a sinusoidal voltage excitation signal to the battery terminals without the need for additional hardware. The impedance spectrum of the battery is calculated based on voltage excitation and current response with the aid of an embedded digital lock in amplifier in a digital signal processor. The measured impedance data are utilized in the application of the complex nonlinear least squares method to extract the battery parameters of the equivalent circuit. These parameters are then compared with the reference values to reach a diagnosis. A prototype of the proposed charger is applied to four valve-regulated lead–acid batteries to measure AC impedance. The results are discussed.

Key words: Equivalent Circuit Parameter, EIS, Intelligent Charger, Online Battery Diagnosis, SOH Online Estimation

I. INTRODUCTION

Lead–acid batteries are popularly adopted as an energy storage element in battery-based applications because of their reliability and affordability [1]-[7]. Battery performance affects the product's reliability and lifetime. Thus, the state of health (SOH) of batteries should be assessed to avoid possible replacement costs caused by sudden system failures. Battery SOH during regular usage also provides information on maintenance scheduling and replacement. However, batteries are chemical energy storage devices that deteriorate over time and eventually reach their end of life. Thus, determining an appropriate replacement time is difficult. Battery SOH must be extensively investigated to improve system reliability.

Manuscript received Aug. 30, 2015; accepted Apr. 30, 2016
Recommended for publication by Associate Editor Hao Ma.
†Corresponding Author: cwj777@ssu.ac.kr
Tel: +82-2-820-0652, Fax: +82-2-817-7961, Soongsil University
*Department of Electrical Engineering, Soongsil University, Korea
**Department of Economics, Soongsil University, Korea

Battery SOH is defined as the relative ratio of the battery capacity at its current state to the nominal capacity when it was new [8], [9]. Previous research has determined that battery SOH is strongly dependent on several factors, such as depth of discharge, temperature variations, and rate of charge/discharge current [10], [11]. The estimation of battery SOH is complex because of the nonlinear relationship between battery SOH and the aforementioned factors. Various methods to estimate SOH have been proposed [12], [13]. An example is the coulomb counting method that estimates battery SOH by counting the maximum available charge of the battery [12]. However, this method cannot be applied during operation because the battery needs to be fully charged and discharged for coulomb counting. Another method is the extended Kalman filter that performs online estimation of the state of charge (SOC) and SOH [13]. This method facilitates the accurate estimation of SOH. However, such method requires a complex estimation algorithm and an accurate model of the battery to obtain reliable results. In addition, estimation accuracy decreases as the battery degrades because the parameters of the equivalent circuit model of the battery vary according to the age of the

battery.

Recent research has indicated that battery impedance variation can be a useful tool to investigate battery aging [13], [14]. Several commercially available battery testers diagnose battery aging by measuring the AC impedance of batteries at a frequency of 1 kHz on the basis of the fact that the real part of the complex impedance of a battery at 1 kHz is almost equal to its ohmic resistance [15], [16]. However, the method may lead to inaccurate internal resistance calculations because ohmic resistance does not always match the real part of the impedance at 1 kHz; this inaccuracy may lead to inaccurate internal resistance calculations, which affect aging estimation. In addition, given that battery SOH must be evaluated periodically, such methods are labor intensive and time consuming, particularly for large battery systems.

If the battery diagnosis function can be integrated into the charger, then the reliability of the system can be improved significantly because battery SOH can be periodically monitored [17], [18]. In addition, the cost associated with the maintenance can be greatly reduced if the battery SOH is monitored automatically and regularly.

Recently, in [19], a novel intelligent charger with an embedded diagnosis function was proposed. With the proposed charger, the standard constant current/constant voltage (CC/CV) method was applied in the current study to charge a lead–acid battery in the normal charge mode, and impedance spectroscopy (EIS) was performed with the sinusoidal voltage excitation generated by the voltage controller in the diagnosis mode. The measured current and voltage were used to calculate the impedance spectrum of the battery by using a digital lock-in amplifier (DLIA). With a complex nonlinear least squares fitting method, the parameters for the equivalent circuit of the lead–acid battery were obtained. Comparison of these parameters with those of a fresh lead–acid battery indicated that battery SOH can be estimated. The proposed method can be implemented in any type of bidirectional charge converter without any extra hardware. As a result, the proposed method requires no additional costs.

II. SOH OF A LEAD–ACID BATTERY BY USING EIS AND ITS EQUIVALENT CIRCUIT MODEL

A. Electrochemical Impedance Measurement Method

The electrochemical impedance of a battery is a complex quantity that represents the battery's current state [20]-[24]. It is an effective modeling and diagnosis tool for electrochemical power sources, such as batteries, fuel cells, and supercapacitors. In [20], various methods to measure the electrochemical impedance of batteries were presented. However, most commercially available EIS instruments are expensive and only suitable for measuring the impedance of single cells or small modules [25], [26]; these drawbacks limit the use of these instruments in research and development.

The impedance spectroscopy measurement of a battery can be performed by applying a small excitation signal at a frequency of interest to the battery and then observing the response signal. Notably, the frequency of interest can be varied within a suitable range to obtain a useful impedance spectrum for the battery. In addition, the response signal generally possesses the same frequency and shape as the excitation signal, but it shows a shift in phase. Based on the current response and voltage excitation, battery impedance is determined as

$$Z(f)=\frac{V(f)}{I(f)}, \tag{1}$$

where

Z(f): impedance of the battery at frequency f,

V(f): voltage excitation (or response) at frequency f,

I(f): current response (or excitation) at frequency f.

The responses of a battery with respect to perturbation signals differ depending on the state of the battery. Therefore, the electrochemical impedance determined with Eq. (1) can be utilized to determine the state of the battery.

As previously mentioned, excitation and response signals are typically small (in the scale of millivolts or milliamps); hence, measurement requires filtering out all unexpected signals and noises. In the current study, a DLIA was adopted to extract the signals at the frequency of interest. This DLIA is preferable because of its high performance in measuring small signals regardless of the high level of noise [27].

An AC signal superimposed on a DC signal and noises, u(n), can be represented in a discrete form as

$$X[n]=DC+A\sin\left(2\pi\frac{f}{f_s}n+\theta\right)+u(n);n=0,1,2,... \tag{2}$$

The DLIA generates two orthogonal sinusoidal reference signals at each frequency as excitation signals generated numerically as Eq. (3). These numeric reference signals are immune to noise [28].

$$\begin{aligned} S[n]&=\sin\left(2\pi\frac{f}{f_s}n\right), \quad n=0,1,2,...,... \\ C[n]&=\cos\left(2\pi\frac{f}{f_s}n\right), \quad n=0,1,2,...,.. \end{aligned} \tag{3}$$

The in-phase and quadrature-phase quantities are obtained by multiplication of the measured signal and sine and cosine reference signals, respectively.

$$I[n]=X[n]\times S[n]=\frac{A}{2}\cos(\theta)+AC \text{ components} \tag{4}$$

$$Q[n]=X[n]\times C[n]=\frac{A}{2}\sin(\theta)+AC \text{ components} \tag{5}$$

By applying a moving average filter to eliminate the AC components in Eqs. (4) and (5), the target signal can be extracted with the magnitude determined in Eq. (6) and the phase determined in Eq. (7).

$$x = 2 \times I[n] \approx A\cos(\theta)$$
$$y = 2 \times Q[n] \approx A\sin(\theta) \quad (6)$$

$$M = \sqrt{x^2 + y^2} = A \; ; \qquad Ph = \tan^{-1}(\frac{y}{x}) = \theta \quad (7)$$

The complex form of the battery impedance can be determined with Eqs. (8) to (9).

$$Z(\omega_0) = R(\omega_0) + jX(\omega_0) \quad (8)$$

$$R(\omega_0) = \frac{V_x I_x + V_y I_y}{I_x^2 + I_y^2}; \; X(\omega_0) = \frac{V_y I_x - V_x I_y}{I_x^2 + I_y^2} \quad (9)$$

Typically, the perturbation signal is swept within the desired frequency range (from 0.1 Hz to 1.0 kHz in this study), after which the impedance data are calculated. The parameters of the equivalent circuit of the lead–acid battery is then obtained based on the obtained impedance data.

B. SOH Estimation Using Extracted Parameters from Electrochemical Impedance

A popular equivalent circuit model of a lead–acid battery is shown in Fig. 1 [29]-[31]. All the electrochemical reactions in a lead–acid battery can be represented by the elements in this equivalent circuit model. R_s is the ohmic resistance that reflects the conductivity of the electrolyte and electrical pathway. R_{ct} and C_{dl} are charge transfer resistance and double layer capacitance, respectively, which describe the transient behaviors caused by the charge transfer reaction. Z_W is the Warburg impedance that reflects battery diffusion. Aside from usage, batteries age because of chemical processes, such as anodic corrosion, positive active mass degradation, irreversible formation of lead sulfate in active mass, short circuits, and loss of water [32]. These processes result in changes in equivalent circuit parameters.

Battery aging is accompanied by an increase in ohmic resistance and a decrease in capacity. If these parameters can be extracted from the impedance spectrum, SOH can be estimated based on variations in parameter values in the equivalent circuit of the battery over the aging process. A method to estimate the SOH of an arbitrary battery using the parameters of its equivalent circuit was introduced in [13]; the equivalent circuit parameters of a battery in fresh and fully aged conditions were used to estimate SOH.

The SOH of an arbitrary battery may also be estimated using its ohmic resistance, as shown in Eq. (10) [13].

$$SOH_{arbitrary} = \left| \frac{R_s^{selected} - R_s^{aged}}{R_s^{fresh} - R_s^{aged}} \right| \quad (10)$$

where

$R_s^{selected}$: ohmic resistance of the battery under test (Ω)

R_s^{fresh} : ohmic resistance of the fresh battery (Ω)

R_s^{aged} : ohmic resistance of the fully aged battery (Ω)

However, Eq. (10) is only valid under the assumption that the relationship between the increase in ohmic resistance and the remaining capacity is linear.

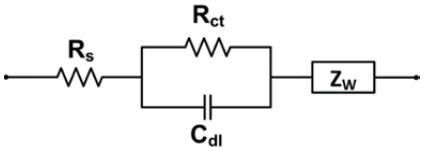

Fig. 1. Equivalent circuit model of a lead–acid battery.

In [27], an advanced method to estimate the life span of a fuel cell by using its cathode time constant (a product of cathode resistance and capacitance) was introduced. Unlike the method in [13], this advanced method does not require strict linearity in the variation of the parameters of the battery equivalent circuit.

In this study, the least squares algorithm was used to determine the equivalent parameters from the best-fit curve of the model data to the measured data. Given that impedance data show a complex form, a complex nonlinear least squares (CNLS) fitting method was adopted to extract the battery parameter values. The CNLS method is a Levenberg–Marquardt least squares method applied to complex numbers. The equivalent circuit model of the battery in Fig. 1 and actual impedance data are the inputs to this method [33]. This method finds the best-fit curve with the model parameters by minimizing the error between the measured and model curves through iterative calculation.

The equivalent circuit model of the battery in Fig. 1 has complex impedance as a function of frequency and parameters, as demonstrated in Eq. (11).

$$Z(\omega) = f(\omega; \theta_i); \quad \theta_i = R_s, R_{ct}, C_{dl}, Z_W \quad (11)$$

In Eq. (11), R_s, R_{ct}, C_{dl}, and Z_W are the parameters of the equivalent circuit model for the lead–acid battery estimated by minimizing the function "Φ".

$$\Phi = \sum_{i=1}^{n} \left[\mathrm{Re}(y_i - Z_i)^2 + \mathrm{Im}(y_i - Z_i)^2 \right] \quad (12)$$

The Taylor series method can calculate impedance based on the previous impedance value and the variations in the approximated parameters. The estimated parameters can be updated with variation Δ by using Taylor series expansion, as shown in Eq. (13).

$$Z(\omega)_{j+1} = Z(\omega)_j + \frac{\partial Z(\omega)_j}{\partial \theta_i} \Delta\theta_i, \quad i = 1,2,3,4 \quad (13)$$

The values of ΔR_s, ΔR_{ct}, ΔC_{dl}, and ΔZ_W are then determined with Eq. (14).

$$\Delta\theta = A^{-1}.G \quad (14)$$

where

$$A = \left[(Z_R)^T.Z_R + (Z_I)^T.Z_I \right]$$
$$G = \left[(Z_R)^T.\Delta y_R + (Z_I)^T.\Delta y_I \right]$$
$$[Z_R]_{ij} = \mathrm{Re}\left(\frac{\partial Z_i}{\partial \theta_i} \right); \qquad [Z_I]_{ij} = \mathrm{Im}\left(\frac{\partial Z_i}{\partial \theta_i} \right) \quad (15)$$
$$[\Delta y_R]_j = \mathrm{Re}(Y_i - Z_i); \quad [\Delta y_I]_j = \mathrm{Im}(Y_i - Z_i)$$

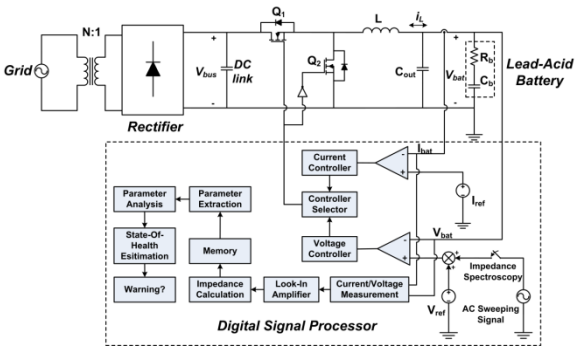

Fig. 2. Block diagram of the proposed intelligent charger.

The abovementioned fitting algorithm can be implemented by an iterative loop in a digital signal processor (DSP). The model parameters R_s, R_{ct}, C_{dl}, and Z_W are initialized in the first loop. In the next iteration, all model parameters are updated based on the calculations. When the value of Φ converges to a certain limit, that is, 10^{-6} in this study, the value that best fits the battery model parameters is obtained [34].

III. Structure and Operation of the Proposed Intelligent Charger with an Embedded Battery Diagnosis Function

Fig. 2 illustrates a block diagram of the proposed intelligent charger with an embedded diagnosis function that uses online impedance spectroscopy. The charger is composed of a bidirectional DC/DC converter and a DSP controller that implements both CC/CV charge and battery diagnosis function using EIS. We used a low-frequency transformer and a non-isolated bidirectional converter for simple structure. Nevertheless, other types of bidirectional converters, including high-frequency transformers, can be used in high-power applications with galvanic isolation without limitations.

The proposed charger has two different operating modes (Fig. 3). In the charge operation, the CC/CV charging method is applied to fully charge a battery. Thereafter, the impedance spectroscopy method is applied to investigate the impedance spectrum of the battery.

To limit the maximum charge current, the battery was initially charged in the CC mode with the rated value (i.e., C/10 in this case) from its specification recommended by the manufacturer. When the battery voltage reached 14.4 V, the CV mode was applied to the battery until the charge current decreases to the cut-off value (i.e., 0.02 C in this case).

After the battery was fully charged, it was allowed to rest for 2 hours to obtain the steady state in terms of charge, concentration, and temperature before EIS measurement [35].

To determine the impedance spectrum of the battery, the battery was excited by a small voltage perturbation generated by the voltage controller of the charger; the current response was measured [36]. The AC impedance of the battery at the

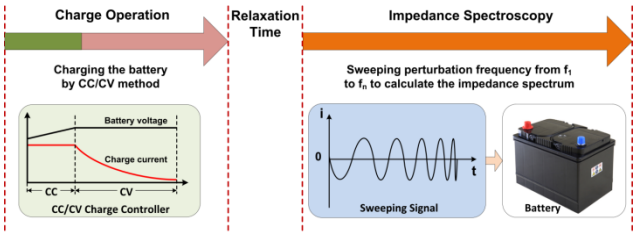

Fig. 3. Operation of the proposed intelligent charger.

frequency of interest was effectively extracted by the DLIA embedded in the DSP. In one cycle of perturbation, the battery was charged and discharged equally through the bidirectional converter. Therefore, the charge inside the battery remained the same before and after the test, thereby ensuring the validity of the test. The parameters of the equivalent circuit for the lead–acid battery were obtained with the CNLS method. These parameters were then used to estimate SOH by comparing the parameter values of an aged lead–acid battery with those of a fresh one. When the measured impedance of the battery showed a larger increase than previous results or reached the values of a fully aged battery, the system generated a warning signal for the user to check the battery. As SOH can be monitored automatically and periodically by using the proposed charger, sudden failures of the battery can be avoided. System reliability also increases, thus reducing the cost of possible replacements and maintenance because of sudden battery-related system failures.

IV. Design of the Digital Controller for the Charger and EIS Function

The converter employed in the proposed charger must be bidirectional to generate perturbations for the EIS of a lead–acid battery. During EIS operation, the battery was charged and discharged for half a cycle at the test frequency. The battery charge state must remain unchanged before and after the impedance spectroscopy test; otherwise, the battery parameters would vary. To charge the lead–acid battery from the grid, a buck topology was selected for the charge converter to step down DC-link voltage to the battery voltage. A bidirectional converter (Fig. 2 [37]) can be derived when the freewheeling diode in the buck converter is replaced by an active switch. The specifications of the charge converter are shown in Table I.

The control-to-output voltage (G_{vd}) and control-to-inductor current (G_{id}) transfer functions were derived with a small-signal modeling technique [38] with a simplified R–C model of the lead–acid battery.

$$G_{vd} = \frac{V_{bus} \times (R_b C_b s + 1)}{s^3 L R_b C_b C_{out} + s^2 L (C_b + C_{out}) + s R_b C_b + 1} \quad (16)$$

$$G_{id} = \frac{V_{bus} \times \left[C_{out} C_b R_b s^2 + (C_b + C_{out}) s \right]}{s^3 L R_b C_b C_{out} + s^2 L (C_b + C_{out}) + + s R_b C_b + 1} \quad (17)$$

TABLE I
SPECIFICATIONS OF THE CHARGE CONVERTER

Parameter	Abbreviation	Value
Power rating	P	60 W
Switching frequency	f_{sw}	60 kHz
Input voltage	V_{bus}	30 V
Output voltage	V_o	14.4 V
Output current	I_{out}	4.0 A
Current ripple	ΔI_L	0.8 A
Output inductor	L	160 µH
Output capacitor	C_{out}	10.0 µF
Output ripple	%	< 2%

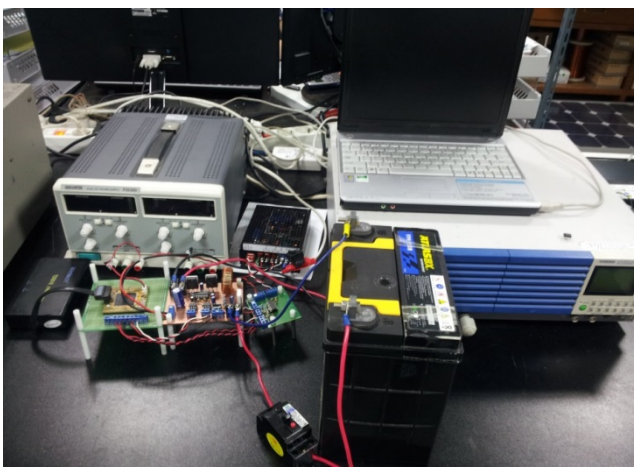

Fig. 4. Experimental setup for the performance test of the proposed intelligent charger.

To obtain high-accuracy impedance results, the crossover frequency should be sufficiently high to generate a pure sinusoidal perturbation. Thus, the bandwidth of the closed loop system was set to be 10 times higher than the highest frequency perturbation. Since the useful impedance spectrum for the lead–acid battery in the proposed method ranges from 0.1 Hz to 1 Khz, the bandwidth of the voltage loop must be higher than 10 KHz. To attenuate the high-frequency switching components on the closed-loop system, the bandwidth of the closed-current loop system was set to 3 KHz, which is much lower than the switching frequency.

V. EXPERIMENTAL RESULTS OF THE PROPOSED INTELLIGENT CHARGER

Fig. 4 shows the experimental setup of the proposed system, which consists of a DC power supply, a 12 V 40 Ah lead–acid battery (ITX40) from the ATLASBX Battery Company [39], and the proposed charger.

The control algorithms, including CC/CV charge and diagnosis functions, were implemented in a high-performance DSP (TMS320F28335) from Texas Instruments. Fig. 5 shows

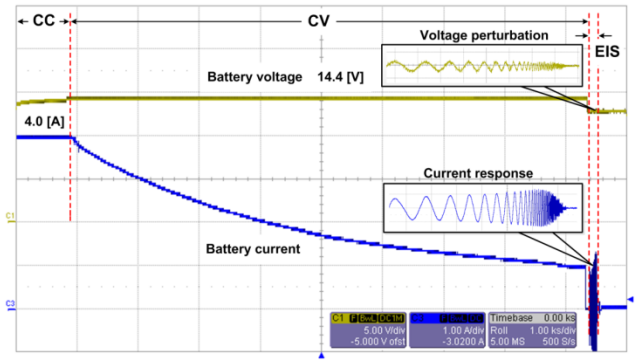

Fig. 5. Charge and EIS operation of the proposed intelligent charger.

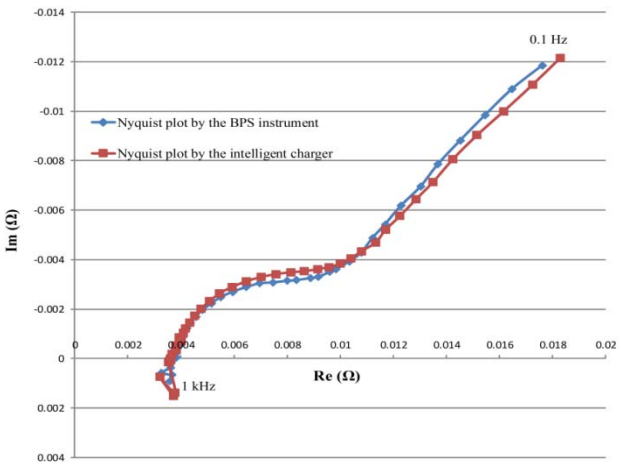

Fig. 6. Comparison of the Nyquist impedance plots of the lead–acid battery obtained by the proposed intelligent charger and the BPS instrument.

the CC/CV charge profile of the lead–acid battery obtained by the proposed charger. The lead–acid battery began to get charged in CC mode with its rated charge current (4.0 A, 0.1 C). When the battery voltage reached the maximum charge voltage of 14.4 V, CV mode was applied until the charge current decreased to 0.8 A (0.02 C), which indicated that the battery was fully charged. The battery was allowed to rest for 2 hours. Afterward, EIS investigation of the lead–acid battery was performed. By adding a small sinusoidal perturbation to the reference of the voltage controller, a voltage excitation was generated and injected to the battery terminal.

To verify the accuracy of the impedance measured by the proposed charger, we compared the results obtained with the proposed charger with those obtained with a commercial EIS instrument (BPS instrument, Kumho). As shown in Fig. 6, the two sets of results differed slightly, and the chi-square value was 0.91%, which indicates a strong correlation between the two results. The proposed charger was then used to measure the impedances of four similar batteries in different SOH states. Three of the batteries were obtained from an electric vehicle (EV) racing club belonging to the Engineering School of Soongsil University, Seoul, Korea (Fig. 7). These batteries

Fig. 7. Four valve-regulated lead–acid batteries used for SOH investigation.

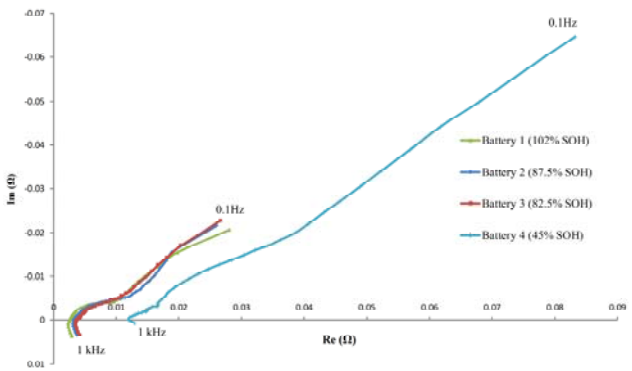

Fig. 8. Nyquist plots of the sample batteries obtained by the intelligent charger.

were valve-regulated lead–acid batteries (DF80L) manufactured by Delkor Corporation; their nominal voltage and capacity were 12.0 V and 80 Ah, respectively [40]. The fourth battery was a brand-new unit with the same specifications from the same manufacturer.

The three batteries had been used in the same EV under different cycles, periods, and conditions. A record of usage history was unavailable. The fresh battery was labeled as 1, whereas the three aged batteries were labeled as 2, 3, and 4.

To measure the SOH of the batteries, we fully charged all the batteries under CC/CV mode charging and then calculated the ampere–hour capacity with the coulomb counting method while discharging the batteries to the cut-off voltage. All four batteries had 102%, 87.5%, 82.5%, and 45% SOH at room temperature. Battery impedance was then measured with the proposed charger. The EIS operation was performed for all four batteries to determine the variation in the ohmic resistance and the other parameters of the equivalent circuit model for the batteries. Fig. 8 shows the Nyquist plots of the four batteries. The impedance plots of batteries 1 to 3 are similar in shape. However, they tend to shift to the right on the real axis, indicating increments in the ohmic resistance (R_s in Fig. 1) of the batteries. The extracted parameter values are listed in Table II. The ohmic resistances of batteries 1 to 4 were 2.13, 2.97, 3.43, and 12.43 mΩ. Fig. 9 shows that the

TABLE II
EXTRACTED PARAMETERS OF THE BATTERY EQUIVALENT CIRCUIT MODELS BY USING THE PROPOSED CHARGER

	Battery 1 (102% SOH)	Battery 2 (87.5% SOH)	Battery 3 (82.5% SOH)	Battery 4 (45% SOH)
R_s (mΩ)	2.13	2.97	3.43	12.43
R_{ct} (mΩ)	2.80	2.44	1.84	3.96
C_{dl} (F)	4.25	7.21	10.17	6.14
Z_W	44.78	43.19	44.9	44.2

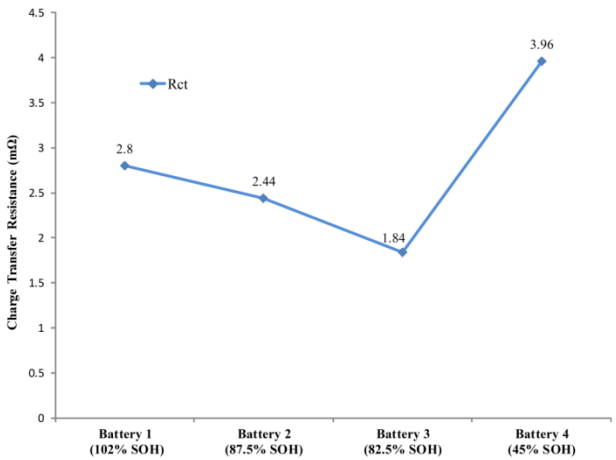

Fig. 9. Ohmic resistance values of the sample batteries.

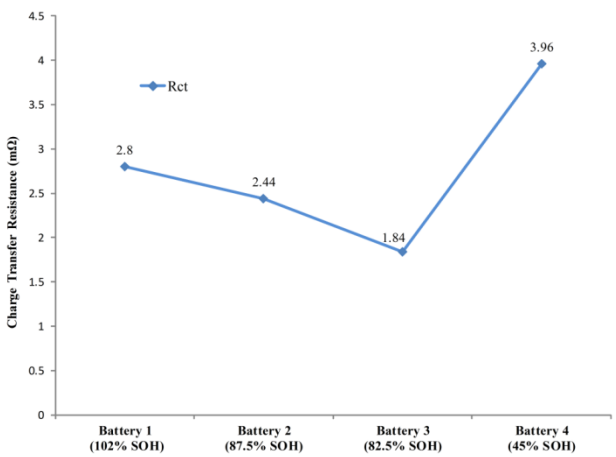

Fig. 10. Charge transfer resistances of the sample batteries.

ohmic resistance R_s value increases as the capacity decreases and significantly, increases as the battery becomes fully aged. However, as the relationship between ohmic resistance and battery capacity is not linear, applying Eq. (10) to calculate the exact value of battery capacity is impossible.

The relationship between battery capacity and the other parameters was also investigated. Warburg impedance was excluded from this investigation because its value varied only slightly for each battery. Figs. 10 and 11 show the variations in the charge transfer resistance and double layer capacitance of each battery. Considering that the variations are nonlinear

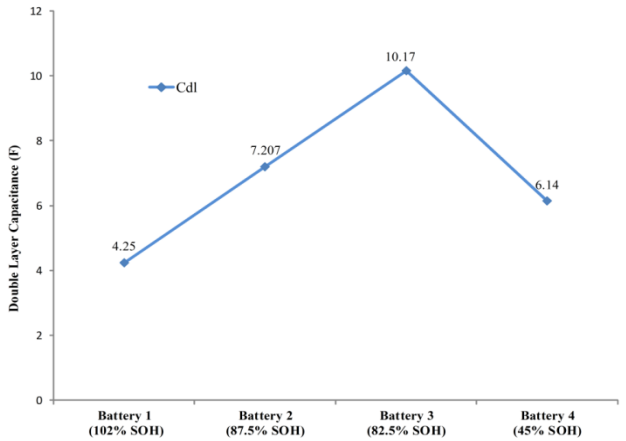

Fig. 11. Double layer capacitances of the sample batteries.

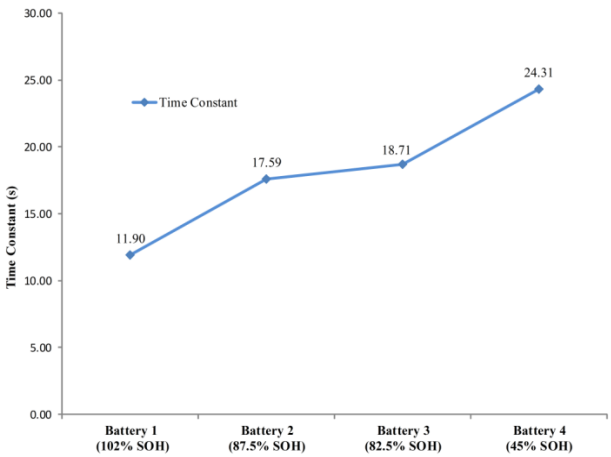

Fig. 12. Time constant values of the sample batteries.

with respect to capacity, these parameters cannot be utilized to estimate battery capacity. Therefore, obtaining the accurate relationship between parameter variations and battery capacity using a single parameter of the battery equivalent circuit model is impossible.

A method to estimate the lifetime of electrochemical energy sources by using the time constant was recommended in [41]. The time constant, a product of the charge transfer resistance and double layer capacitance of the equivalent circuit model, ultimately indicates the electrochemical reaction rate occurring inside an electrochemical energy device. Fig. 12 shows the variation in the time constant for each battery. Evidently, the time constant increases as the battery ages. This trend suggests that the time constant may be used as a reliable indicator of battery aging, as the relationship between variations in parameter value and capacity is linear (Fig. 12). However, because this test only used four batteries, we cannot sufficiently argue that the capacity or SOH can be determined by detecting variations in the aforementioned parameter value. To obtain the accurate relationship between the capacity and parameter variations, more batteries must be tested in future research. Nevertheless, the proposed charger can periodically measure the time constant of a battery, compare it with a reference value, and generate a warning for users to check the battery before it reaches the critical condition. The proposed charger can also significantly reduce the maintenance costs of battery-based systems, thereby increasing system reliability.

VI. Conclusions

A novel intelligent battery charger with an embedded battery diagnosis function using online impedance spectroscopy was proposed. The impedance spectrum of a lead–acid battery can be measured, and any variation in impedance can be detected successfully with the proposed charger. Given that the proposed method can be implemented with no additional hardware, the cost of the proposed charger relative to that of conventional chargers is low. With the proposed charger, battery SOH can be monitored automatically and periodically, and sudden battery failures can be avoided. The use of the proposed charger also increases the reliability of battery-based systems and reduces the costs for replacement and maintenance.

Acknowledgment

This work was supported by the Soongsil University Research Fund (2013).

References

[1] M. Yekini Suberu, M. Wazir Mustafa, and N. Bashir, "Energy storage systems for renewable energy power sector integration and mitigation of intermittency," *Renewable and Sustainable Energy Reviews,* Vol. 35, pp. 499-514, Jul. 2014.

[2] B.-H. Lee, D.-H. Shin, H.-S. Song, H. Heo, and H.-J. Kim, "Development of an advanced hybrid energy storage system for hybrid electric vehicles," *Journal of Power Electronics,* Vol. 9, No. 1, pp. 51-59, Jan. 2009.

[3] S.-H. Han, H.-G. Kim, H. Cha, T.-W. Chun, and E.-C. Nho, "Bi-directional multi-level converter for an energy storage system," *Journal of Power Electronics,* Vol. 14, No. 3, pp. 499-506, May 2014.

[4] D.-H. Jang and S.-K. Han, "Low cost high power density photovoltaic power conditioning system with an energy storage system," *Journal of Power Electronics,* Vol. 12, No. 3, pp. 487-494, May 2012.

[5] C. Bussar, M. Moos, R. Alvarez, P. Wolf, T. Thien, H. Chen, Z. Cai, M. Leuthold, D.U. Sauer, and A. Moser, "Optimal allocation and capacity of energy storage systems in a future european power system with 100% renewable energy generation," *Energy Procedia*, Vol. 46, pp. 40-47, 2014.

[6] H. Jung, H. Wang, and T. Hu, "Control design for robust tracking and smooth transition in power systems with battery/supercapacitor hybrid energy storage devices," *Journal of Power Sources*, Vol. 267, pp. 566-575, Dec. 2014.

[7] H. Jia, Y. Mu, and Y. Qi, "A statistical model to determine

the capacity of battery–supercapacitor hybrid energy storage system in autonomous microgrid," *International Journal of Electrical Power & Energy Systems*, Vol. 54, pp. 516-524, Jan. 2014.

[8] C. Weng, Y. Cui, J. Sun, and H. Peng, "On-board state of health monitoring of lithium-ion batteries using incremental capacity analysis with support vector regression," *Journal of Power Sources*, Vol. 235, pp. 36-44, Aug. 2013.

[9] W. Waag and D. U. Sauer, "Secondary Batteries – Lead–Acid Systems | State-of-Charge/Health," in *Encyclopedia of Electrochemical Power Sources,* J. Garche (Ed.), Elsevier, Amsterdam, pp. 793-804, 2009.

[10] S. S. Choi, and H. S. Lim, "Factors that affect cycle-life and possible degradation mechanisms of a Li-ion cell based on LiCoO2," *Journal of Power Sources*, Vol. 111, No. 1, pp. 130-136, Sep. 2002.

[11] J. R. Belt, C.D. Ho, T. J. Miller, M. A. Habib, and T. Q. Duong, "The effect of temperature on capacity and power in cycled lithium ion batteries," *Journal of Power Sources*, Vol. 142, No. 1-2, pp. 354-360, Mar. 2005.

[12] K. S. Ng, C.-S. Moo, Y.-P. Chen, and Y.-C. Hsieh, "Enhanced coulomb counting method for estimating state-of-charge and state-of-health of lithium-ion batteries," *Applied Energy*, Vol. 86, No. 9, pp. 1506-1511, Sep. 2009.

[13] K. Jonghoon, L. Seongjun, and B.H. Cho, "Complementary Cooperation Algorithm Based on DEKF Combined With Pattern Recognition for SOC/Capacity Estimation and SOH Prediction," *IEEE Trans. Power Electron.*, Vol. 27, No. 1, pp. 436-451, Jan. 2012.

[14] H. Blanke, O. Bohlen, S. Buller, R.W. De Doncker, B. Fricke, A. Hammouche, D. Linzen, M. Thele, and D.U. Sauer, "Impedance measurements on lead–acid batteries for state-of-charge, state-of-health and cranking capability prognosis in electric and hybrid electric vehicles," *Journal of Power Sources*, Vol. 144, No. 2, pp. 418-425, Jun. 2005.

[15] Y. Zhan, H. Wang, and J. Zhu. "Modelling and control of hybrid UPS system with backup PEM fuel cell/battery," *International Journal of Electrical Power & Energy Systems*, Vol.43, No. 1, pp. 1322-1331, Dec. 2012.

[16] Y.-P. Yang, F.-C. Wang, H.-P. Chang, Y.-W. Ma, and B.-J. Weng, "Low power proton exchange membrane fuel cell system identification and adaptive control," *Journal of Power Sources*, Vol. 164, No.2, pp. 761-771, Feb. 2007.

[17] Thanh-Tuan Nguyen and W. Choi, "Development of the Intelligent Charger with Embedded Battery Diagnosis Function Using Online Impedance Spectroscopy," in *Power Electronics Annual Conference KIPE*, pp. 329-330, 2013.

[18] Van-Tuan Doan, Van-Binh Vu, Hai-Nam Vu, Duc-Hung Tran, and Woojin Choi, "Intelligent charger with online battery diagnosis function," in *9th International Conference on Power Electronics and ECCE Asia (ICPE-ECCE Asia)*, 2015.

[19] Thanh-Tuan Nguyen, Van-Long Tran and Woojin Choi, "Development of the intelligent charger with battery State-Of-Health estimation using online impedance spectroscopy," *23rd International Symposium on Industrial Electronics (ISIE)*, pp. 454-458, 2014.

[20] F. Huet, "A review of impedance measurements for determination of the state-of-charge or state-of-health of secondary batteries," *Journal of Power Sources*, Vol. 70, No. 1, pp. 59-69, Jan. 1998.

[21] L. Jong-Hak and C. Woojin, "Novel State-of-Charge Estimation Method for Lithium Polymer Batteries Using Electrochemical Impedance Spectroscopy," *Journal of Power Electronics*, Vol. 11, No. 2, pp. 237-243, Mar. 2011.

[22] V. Kuznetsov, A. Maljusch, R.M. Souto, A.S. Bandarenka, and W. Schuhmann, "Characterisation of localised corrosion processes using scanning electrochemical impedance microscopy," *Electrochemistry Communications*, Vol. 44, pp. 38-41, 2014.

[23] O.S. Mendoza-Hernandez, H. Ishikawa, Y. Nishikawa, Y. Maruyama, Y. Sone, and M. Umeda, "State of Charge Dependency of Graphitized-Carbon-Based Reactions in a Lithium-ion Secondary Cell Studied by Electrochemical Impedance Spectroscopy," *Electrochimica Acta,* Vol. 131, pp. 168-173, Jun. 2014.

[24] Y. Xie, J. Li and C. Yuan, "Mathematical modeling of the electrochemical impedance spectroscopy in lithium ion battery cycling," *Electrochimica Acta*, Vol. 127, pp. 266-275, 2014.

[25] G. I. Company, *Gamry EIS300 Product Brochure*.

[26] L. WonATech Co., *WEIS500 Electrochemical Workstation*.

[27] C. Woojin and L. Juhyung, "Development of the low-cost impedance spectroscopy system for modeling the electrochemical power sources," in *7th International Conference on Power Electronics ICPE '07*, pp. 113-118, 2007.

[28] J. M. Masciotti, J. M. Lasker, and A. H. Hielscher, "Digital lock-in detection for discriminating multiple modulation frequencies with high accuracy and computational efficiency," *IEEE Trans. Instrum. Meas.,* Vol. 57, No. 1, pp. 182-189, Jan. 2008.

[29] C. Fleischer, W. Waag, H.-M. Heyn, and D.U. Sauer, "On-line adaptive battery impedance parameter and state estimation considering physical principles in reduced order equivalent circuit battery models: Part 1. Requirements, critical review of methods and modeling," *Journal of Power Sources*, Vol. 260, pp. 276-291, Aug. 2014.

[30] D. Andre, M. Meiler, K. Steiner, H. Walz, T. Soczka-Guth, and D. U. Sauer, "Characterization of high-power lithium-ion batteries by electrochemical impedance spectroscopy. II: Modelling," *Journal of Power Sources*, Vol. 196, No. 12, pp. 5349-5356, Jun. 2011.

[31] K. Brik and F. ben Ammar, "Causal tree analysis of depth degradation of the lead acid battery," *Journal of Power Sources*, Vol. 228, pp. 39-46, Apr. 2013.

[32] P. Ruetschi, "Aging mechanisms and service life of lead–acid batteries," *Journal of Power Sources,* Vol. 127, No. 1-2, pp. 33-44, Mar. 2004.

[33] B. A. Boukamp, "A Nonlinear Least Squares Fit procedure for analysis of immittance data of electrochemical systems," *Solid State Ionics,* , Vol. 20, No. 1, pp. 31-44, Feb. 1986.

[34] S. Manoharan, S. Birlasekaran, and C. V. Suryanarayana, "Computer program for nonlinear least square analysis of impedance and admittance data," *Bulletin of Electrochemistry*, Vol. *2*, No. 5, pp. 509-513, 1986.

[35] M. Reichert, D. Andre, A. Rösmann, P. Janssen, H. G. Bremes, D. U. Sauer, S. Passerini, and M. Winter, "Influence of relaxation time on the lifetime of commercial lithium-ion cells," *Journal of Power Sources*, Vol. 239, pp. 45-53, Oct. 2013.

[36] M. A. Danzer and E. P. Hofer, "Electrochemical parameter identification – An efficient method for fuel cell

impedance characterisation," *Journal of Power Sources*, Vol. 183, No. 1, pp. 55-61, Aug. 2008.
[37] H.-M. Ryu, "Highly Efficient High-Voltage MOSFET Converter with Bidirectional Power Flow Legs," *Journal of Power Electronics*, Vol. 14, No. 2, pp. 265-270, Mar. 2014.
[38] R. W. Erickson and D. Maksimovic, *Fundamental of Power Electronics*, 2nd ed., Kluwer Academic, 2001.
[39] A. Company, *ATLASBX ITX Series*.
[40] L. Delkor Corporation, *Delkor Battery DF80L Model*.
[41] J.-H. Lee, J.-H. Lee, W. Choi, K.-W. Park, H. Y. Sun, and J.-H. Oh, "Development of a method to estimate the lifespan of proton exchange membrane fuel cell using electrochemical impedance spectroscopy," *Journal of Power Sources*, Vol. 195, pp. 6001-6007, Mar. 2010.

Thanh-Tuan Nguyen was born in Ninh Binh, Vietnam, in 1987. He received his B.S. and M.S. degrees in mechatronics and electrical engineering from Vietnam National University, Vietnam, and from Soongsil University, Republic of Korea, in 2010 and 2014, respectively. Since November 2014, he has been working for his Ph.D. at UiT, the Arctic University of Norway, Tromsø. His research interests include modeling and control of DC–DC converters for renewable energy sources, hybrid energy storage systems, electric/hybrid electric vehicles, and diagnosis of electrochemical energy sources through electrochemical impedance spectroscopy.

Van-Tuan Doan was born in Hai Phong, Vietnam, in 1985. He received his B.S. and M.S. degrees in electrical engineering from Vietnam Maritime University, Vietnam, in 2008 and 2012, respectively. He is currently pursuing his Ph.D. in electrical engineering at Soongsil University, Republic of Korea. His research interests are DC–DC converters, power factor regulator converters, inverters, and soft-switching techniques for pulse-width modulation converters.

Geun-Hong Lee received his B.S and M.S degrees in electrical engineering from Myongji University, Seoul, Korea, in 1988 and 1995, respectively. He is currently working for his Ph.D. at Soongsil University. His research interests include electric machine control and power conversion.

Hyung-Won Kim was born in Gangwon, Republic of Korea, in 1972. He received his B.S. and M.S. degrees in electrical engineering from Seoul National University of Science & Technology and Soongsil University, Republic of Korea, in 1998 and 2000, respectively. He is currently working for his Ph.D. at Soongsil University. His research interests include switching power converters, power electronic systems, battery management systems, and high-voltage pulse power systems. He is currently a researcher at Crony Inc.

Woojin Choi was born in Seoul, Republic of Korea, in 1967. He received his B.S. and M.S. degrees in electrical engineering from Soongsil University, Republic of Korea, in 1990 and 1995, respectively. He received his Ph.D. in electrical engineering from Texas A&M University, USA, in 2004. He worked with Daewoo Heavy Industries as a research engineer from 1995 to 1998. In 2005, he joined the School of Electrical Engineering, Soongsil University. His research interests include modeling and control of electrochemical energy sources (e.g., fuel cells, batteries, and supercapacitors), power-conditioning technologies in renewable energy systems, and DC–DC converters for fuel cells and hybrid electric vehicles. Dr. Choi is an associate editor of IEEE Transactions on Industry Applications and a publication editor of the Journal of Power Electronics of the Korean Institute of Power Electronics.

Dae-Wook Kim was born in Seoul, Republic of Korea, in 1973. He received his B.A. and Ph.D. degrees in economics from Yonsei University, Republic of Korea, and from the University of California–Davis, USA, in 1999 and 2004, respectively. From 2004 to 2007, he served as a research fellow at the Korea Institute for Industrial Economics and Trade. In 2007, he joined the Department of Economics, Soongsil University. His current interests include energy economics, particularly market structure and competition in energy industries.